Dynamical Aspects of Twin Tropical Cyclones Associated with the Madden–Julian Oscillation

ROSANA NIETO FERREIRA AND WAYNE H. SCHUBERT

Department of Atmospheric Science, Colorado State University, Fort Collins, Colorado

JAMES J. HACK

National Center for Atmospheric Research, Boulder, Colorado

(Manuscript received 22 July 1994, in final form 25 September 1995)

ABSTRACT

A nonlinear shallow-water model on the sphere is used to study barotropic aspects of the formation of twin tropical disturbances by Madden–Julian oscillation (MJO) convection.

In the model, the effect of MJO convection upon the lower-tropospheric tropical circulation was simulated by an eastward moving, meridionally elongated mass sink straddling the equator. The intensity and propagation speed of the mass sink were chosen to simulate observations that MJO convection intensifies while nearly stationary in the eastern equatorial Indian Ocean, weakens while moving eastward over the Maritime Continent, again intensifies once it reaches the west Pacific Ocean, and finally becomes stationary and dies off near the date line. This mass sink produced twin cyclones in the two regions where it was stationary, namely, where it was initially turned on and where it was turned off. In addition, the mass sink produced two zonally elongated cyclonic potential vorticity anomalies straddling the equator in the region where it propagated eastward.

It is proposed that MJO convection produces twin tropical disturbances in the two regions where it is nearly stationary, namely, its region of formation in the eastern Indian Ocean and its region of decay near the date line. Additional tropical disturbances may arise from the breakdown of the elongated shear regions produced by the eastward propagating MJO convection.

In addition, a series of initial value experiments was performed to determine the conditions under which twin cyclones become so strongly coupled that they propagate directly eastward as a cyclone pair. Apparently, such movement requires the cyclones to be so close together that the situation rarely, if ever, occurs in nature.

1. Introduction

Exclusively in the Indian and west Pacific Oceans, there are occasions of nearly simultaneous formation of two tropical cyclones that straddle the equator at about the same longitude and between 10°N and 15°S. These storms are called cross-equatorial tropical cyclone pairs or twin tropical cyclones, reflecting their symmetry about the equator.

In the western Pacific, twin tropical cyclones occur between October and May, with higher frequencies during December through February (Keen 1982). According to the strict definitions of Lander (1990) and Harrison and Giese (1991), the frequency of occurrence of twin tropical cyclones in the western Pacific Ocean is once every 2–5 years. The use of a less strict definition for twin tropical cyclones by Keen (1982, 1988) resulted in a frequency of occurrence of 2.4 events per year. Other sources of variability in climatologies of twin tropical cyclone frequency are differences in periods of time and regions studied as well as data used. In the Indian Ocean, twin tropical cyclones are weaker and harder to document (Lander 1990).

Liebmann et al. (1994) observed that tropical depressions and cyclones in the Indian and western Pacific Oceans preferentially occur during the convective phase of the Madden–Julian oscillation (MJO: Madden and Julian 1971, 1994) to the west of the large-scale convection near the equator. This is expected since, among other factors, tropical cyclogenesis is favored in regions of intense low-level vorticity (Gray 1979) such as the cyclonic Rossby gyres that trail the MJO convection in its eastward movement.

The MJO is a global-scale disturbance of the tropical atmosphere whose period varies between 20 and 80 days, with most frequent occurrence around 45 days (Madden and Julian 1994). Its signal is observed in both the convection and flow fields in the Eastern Hemisphere and only in the flow fields in the Western Hemisphere. The MJO convection follows the semi-

Corresponding author address: Dr. Rosana Nieto Ferreira, Department of Atmospheric Science, Colorado State University, Fort Collins, CO 80523.
E-mail: rosana@bjerknes.atmos.colostate.edu

annual migration of the intertropical convergence zone across the equator, having a weaker signal in the northern summer (e.g., Salby and Hendon 1994).

Observational studies (Rui and Wang 1990; Wang and Rui 1990; Weickman and Khalsa 1990) have shown that during the onset of an MJO episode convection intensifies while remaining practically stationary in the eastern equatorial Indian Ocean. Later, the convection weakens while moving eastward over the Maritime Continent (Indonesia and Malaysia) and again intensifies upon reaching the warm waters of the western Pacific Ocean. Near the date line, the MJO convection becomes stationary and decays. The convective signal of the MJO also possesses a strong standing component in the Indian and western Pacific Oceans (Weickmann and Khalsa 1990; Yasunari 1979).

Nakazawa (1988) found that the MJO convection is composed of a hierarchy of convective scales. At the top of this hierarchy are "super cloud clusters," which are large areas of organized convection with a horizontal scale on the order of 10^3 km and a lifetime between 2 and 10 days. Super cloud clusters typically propagate eastward at speeds that vary between 5 and 15 m s^{-1}. The building blocks of a super cloud cluster are cloud clusters with a horizontal scale on the order of 10^2 km; lifetimes range between 1 and 2 days and typical propagation is to the west (Nakazawa 1988; Lau et al. 1991; Sui and Lau 1992; Mapes and Houze 1993). The eastward propagation of a super cloud cluster is due to the formation of new cloud clusters on its east side and dissipation on the west side.

The circulation pattern forced by MJO convection consists of Rossby gyres and near-equatorial westerly winds to the west of the convection and a Kelvin wave signature to its east. This circulation pattern accompanies the MJO convection as it propagates eastward (at ~5 m s^{-1}) from the Indian Ocean to the west Pacific Ocean. In the west Pacific, a freely propagating Kelvin wave signal emanates from the dying convection and propagates into the Western Hemisphere at a much faster speed.

In recent years, the study of the MJO (e.g., Lau et al. 1989; Weickmann 1991) and tropical cyclones (e.g., Keen 1982, 1988) and their associated equatorial westerly wind bursts (WWBs) has received increased attention due to their possible role in triggering El Niño events. During a WWB, the low-level (surface–700 mb) equatorial winds, which are usually easterly, blow from the west at speeds in excess of 5 m s^{-1}. In the west Pacific, WWBs are most frequent during November through April (Keen 1988), last between 2 and 39 days, and have zonal extent between 5° and 65° (Keen 1988; Harrison and Giese 1991). However, about 60% of all WWBs last between 2 and 4 days and extend through less than 15° of longitude (Keen 1988). In addition to the MJO and its associated super cloud clusters (Nakazawa 1988; Lau et al. 1989; Sui and Lau 1992), other possible mechanisms to produce and intensify WWBs are cold surges originating in the midlatitudes (Love 1985) or the genesis and intensification of tropical cyclones near the equator (e.g., Nitta 1989; Lander 1990; Hartten 1996).

The causal relationships between tropical cyclones, WWBs, and El Niños are not yet well understood. It has been proposed (e.g., Keen 1982, 1988; Luther et al. 1983; Miller et al. 1988; Giese and Harrison 1991) that a series of WWB events may participate in the early stages of an El Niño event by decreasing the easterly trade winds in the central and west Pacific Ocean and triggering oceanic equatorially trapped Kelvin waves, which will cause an increase in sea surface temperature in the eastern and central east Pacific (e.g., Kindle and Phoebus 1995). Giese and Harrison (1991) showed that WWBs are most efficient at producing large-amplitude Kelvin waves when the strongest zonal winds occur at the equator. Since the vast majority of WWBs are related to nearby tropical cyclones (Hartten 1996) and the strongest, longer-lasting, and most horizontally extensive WWBs are often those related to nearby twin tropical cyclones (Keen 1988; Harrison and Giese 1991; Hartten 1996), it is possible that these storms play an important role in triggering El Niño events. For instance, twin tropical cyclones preceeded the 1986–87 (Miller et al. 1983; Nitta 1989; Nitta and Motoki 1987) and 1991–92 (Kindle and Phoebus 1995) El Niño events.

In this study, the possibility that MJO convection may produce several tropical disturbances near the equator will be investigated using a global nonlinear shallow-water model. As previously mentioned, MJO convection forces a horizontal circulation pattern dominated by Rossby gyres to its west and a Kelvin wave signature to its east (e.g., Nakazawa 1988; Liebmann et al. 1994). This circulation pattern has been simulated in a number of numerical studies (e.g., Gill 1980; Gill and Philips 1986; Lau et al. 1989; Raymond 1993; Kuma 1994) as the response forced by near-equatorial large-scale organized convection. The formation of tropical cyclones within each of these gyres ultimately depends on whether the environmental conditions are favorable for tropical cyclogenesis (Gray 1979; Zehr 1993). Since MJO convection is climatologically more stationary and stronger in the eastern Indian and west Pacific Oceans (e.g., Rui and Wang 1990; Wang and Rui 1990; Weickman and Khalsa 1990), it will force stronger tropical circulations in these regions. In this study, experiments using moving and stationary mass sinks of varying intensity in a shallow-water model will be used to study tropical disturbance formation in connection with MJO convection.

The simple experiments discussed in this paper have the advantage of allowing easier understanding of some of the dynamical processes involved in the formation of twin tropical disturbances. The main limitations of this study are imposed by the absence of moist processes, vertical stratification, and underlying varying sea surface temperature, and the use of a resting initial state. These simplifications imply that processes such as the origin, propagation, and decay (e.g., Yamagata

and Hayashi 1984; Hsu et al. 1990; Bladé and Hartmann 1994; Hayashi and Golder 1994; Hu and Randall 1994) of the MJO convection cannot be directly addressed and have to be simulated by a highly simplified mass sink. The horizontal structure of the mass sink used in this paper is a very simple idealization of the MJO convection since it does not take into account its hierarchy of convective scales. The inclusion in these experiments of the smaller scales of convection embedded in the MJO would result in the production of smaller-scale PV features. The inversion of this more detailed PV field would result in smooth circulations much like the ones discussed in this paper. The main advantage of resolving the smaller scales of convection would be that the MJO life cycle and propagation mechanisms could be studied.

This paper is organized as follows. In section 2, three observed cases of twin tropical disturbances in the Indian and west Pacific Oceans are discussed. Section 3 and the appendix review the nonlinear, global, shallow-water model used in this study. A benchmark simulation run with a stationary mass sink centered at the equator is shown in section 4. In section 5, the effects of mass sink movement and intensity variations upon the formation of cyclones[1] are studied. Finally, section 6 presents some results of initial value problems on twin cyclone motion.

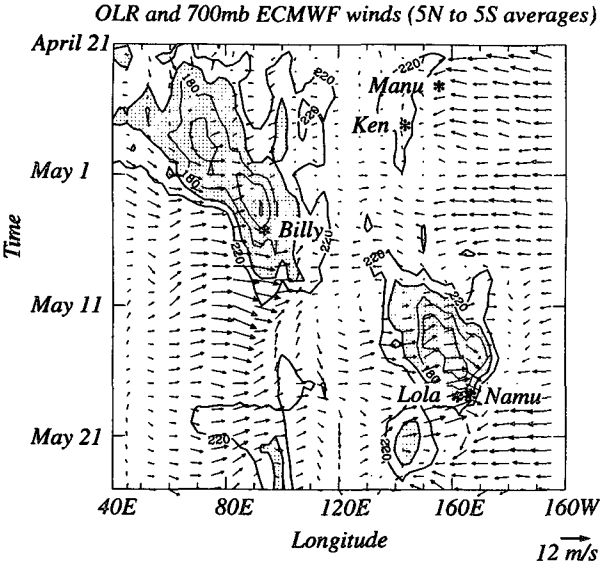

FIG. 1. Time–longitude diagram of ECMWF 700-mb winds and observed daily OLR averaged between 5°N and 5°S in the region between 40° and 160°E and during 21 April–25 May 1986. Areas with OLR lower than 200 W m^{-2} are shaded to indicate convection. Longitudes and dates of formation of five tropical cyclones that formed within three twin tropical disturbances during April and May 1986 are indicated.

2. Observations

In this section a general description of the low-level circulation fields and outgoing longwave radiation (OLR) associated with an MJO event that occurred in April and May of 1986 is presented. This is not intended as a case study and it is offered here simply as a motivation for the shallow-water simulations presented in sections 4 and 5.

Figure 1 shows a time–longitude diagram of European Centre for Medium-Range Weather Forecasts (ECMWF) 700 mb winds and observed daily OLR averaged between 5°N and 5°S in the region between 40° and 160°E and during 21 April through 25 May 1986. Annual and semiannual variations were removed from both time series, and a recursive 1–2–3–2–1 filter[2] was applied. In numerous previous studies OLR has been used as an indicator of convective activity. In Fig. 1, areas with OLR lower than 200 W m^{-2} are stippled to denote convection, and the longitude and dates of formation of five tropical cyclones are indicated. A cross-equatorial super cloud cluster that occurred near 145°E in late April (Fig. 1) was possibly associated with an MJO episode that moved into the west Pacific in late March. An MJO episode began in the western Indian Ocean in late April and reached the west Pacific in mid-May, propagating at a speed of about 7 m s^{-1}. The convection and trailing near-equatorial westerly winds associated with this MJO episode were strong in the eastern Indian and west Pacific Oceans and very weak over the Maritime Continent (between 100° and 140°E, Fig. 1), in good agreement with the findings of Wang and Rui (1990) and Rui and Wang (1990).

Figure 2 shows 5-day-averaged ECMWF 700-mb wind fields and satellite-observed OLR for the period between 21 April and 20 May 1986. Areas with OLR lower than 200 W m^{-2} are again shaded to indicate convection. The two cyclonic shear regions straddling the equator near New Guinea during 21–25 April (Fig. 2a) formed in association with a near-equatorial super cloud cluster (Fig. 1). Twin tropical cyclones Ken and Manu formed in the vicinity of these cyclonic shear regions. Tropical Storm Ken formed near 6°N, 140°E on 26 April and intensified into a typhoon on 27 April (JTWC 1986). Tropical Storm Manu formed on 23 April near 11°S, 154°E (Kingston 1986). Equatorial westerly winds associated with Typhoon Ken reached maximum intensity and horizontal extent during 26–30 April (Fig. 2b) and then gradually weakened as the storm continued on its northwestward movement (Fig. 2c). Easterly winds prevailed in the remainder of the west Pacific Ocean between 21 April and 5 May (Figs. 2a–c).

The onset of an MJO episode occurred during 21–25 April in the tropical Indian Ocean as evidenced by

[1] The term cyclone is hereafter used to designate closed cyclonic circulations.

[2] In the recursive 1–2–3–2–1 filter each smoothed value is the central point of a five-point weighted average in which the weights are 1, 2, 3, 2, and 1, respectively, from the first to the last point.

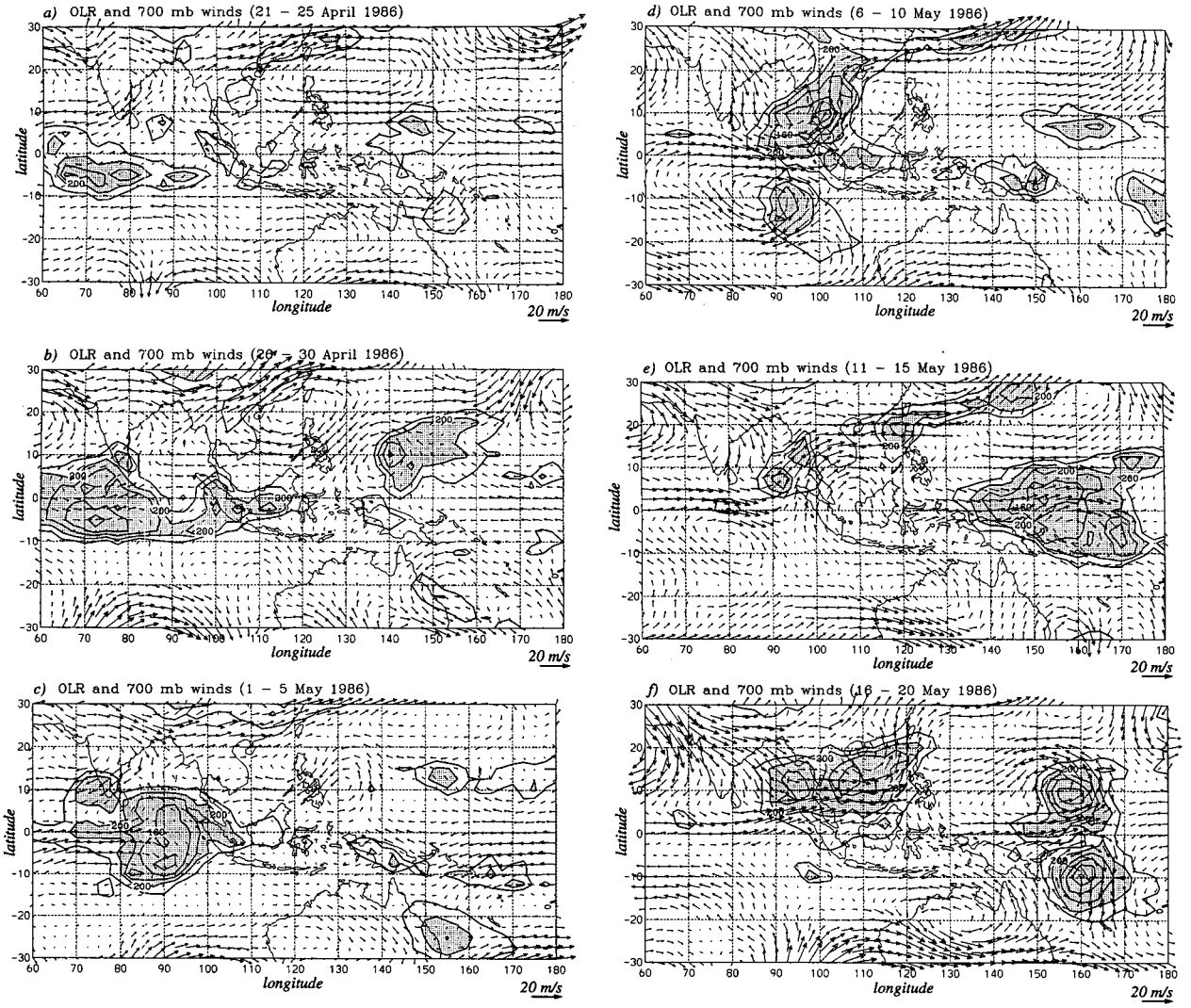

FIG. 2. Five-day-averaged OLR and ECMWF 700-mb wind fields for the period between 21 April and 21 May 1986. Areas with OLR lower than 200 W m^{-2} are shaded to indicate convection.

the broad region of convection and weak equatorial westerly winds ($\sim$3 m s^{-1}) in Fig. 2a. The areal extent and intensity of the convection and equatorial westerlies progressively increased, and by 1–5 May (Fig. 2c), two cyclonic circulations straddled the equator just to the west of the convection. In the Northern Hemisphere (NH) a cyclonic circulation was centered near 5°N, 80°E, and in the Southern Hemisphere (SH) a zonally elongated monsoon trough was centered near 10°S. Tropical Cyclone Billy formed on the easternmost side of this monsoon trough (near 6°S, 92°E) on 5 May (Kingston 1986). No corresponding tropical cyclone twin formed in the NH cyclonic circulation. During 6–10 May (Fig. 2d) convection in the Indian Ocean weakened, and equatorial westerlies peaked (maximum 5-day average of 14 m s^{-1}) in association with Tropical Cyclone Billy in the SH. Averaged equatorial westerlies in excess of 5 m s^{-1} prevailed in the Indian Ocean during 26 April through 20 May, indicating the occurrence of WWBs. During that period most of the MJO convection and the strongest westerly winds were centered in the SH.

Meanwhile in the west Pacific, equatorial easterlies weakened west of about 165°E as the MJO convection set in. During 11–15 May (Fig. 2e), a large region of convection and strong westerly winds centered in the NH dominated the equatorial west Pacific. WWBs with maximum 5-day-average winds of 12 m s^{-1} dominated the west Pacific, and two regions of cyclonic circulation straddled the equator between 140° and 160°E. During 16–20 May (Fig. 2f), twin tropical cyclones Lola and Namu formed in the western Pacific within the aforementioned cyclonic circulations. Tropical Storm Lola became a typhoon on 17 May at 8°N, 160°E (JTWC

1986), and Tropical Storm Namu became a tropical cyclone on 17 May at about 8°S, 163°E (Kingston 1986). Typhoon Lola and Tropical Cyclone Namu contributed to strengthening the equatorial westerlies, which later weakened and moved westward as the storms moved poleward and westward. Easterly winds again dominated the equatorial west Pacific after 22 May (Fig. 1).

In at least two of the cases of twin tropical disturbance formation discussed above, the convective phase of an MJO event was present at the region of formation. Another example of consecutive formation of twin tropical disturbances in the Indian and west Pacific Ocean occurred in 1984 during November and December. However, not all cases of twin tropical cyclones are related to MJO convection. For instance, twin tropical cyclones Roger and Irma formed in March of 1993 in association with a stationary super cloud cluster that was independent of any MJO episodes (Flatau et al. 1995).

3. The shallow-water equations

A spectral shallow-water model on the sphere will be used in sections 4–6 to study the formation of the cyclonic circulations of twin tropical disturbances and the movement of twin cyclones. The shallow-water equations are

$$\frac{\partial u}{\partial t} - \zeta v + \frac{\partial\left[gh + \frac{1}{2}(u^2 + v^2)\right]}{a\cos\phi\,\partial\lambda} = 0, \quad (1)$$

$$\frac{\partial v}{\partial t} + \zeta u + \frac{\partial\left[gh + \frac{1}{2}(u^2 + v^2)\right]}{a\partial\phi} = 0, \quad (2)$$

$$\frac{\partial h}{\partial t} + \frac{\partial(hu)}{a\cos\phi\,\partial\lambda} + \frac{\partial(hv\cos\phi)}{a\cos\phi\,\partial\phi} = Q, \quad (3)$$

where

$$\zeta = 2\Omega\sin\phi + \frac{\partial v}{a\cos\phi\,\partial\lambda} - \frac{\partial(u\cos\phi)}{a\cos\phi\,\partial\phi} \quad (4)$$

is the absolute vorticity. Here, u and v are the eastward and northward components of velocity, h is the fluid depth, a is the radius of the earth, Q is a mass sink or source, and λ and ϕ are longitude and latitude, respectively. Equations (1)–(3) form a closed system in u, v, and h. Model integration is based on the spectral method and is actually performed on the divergence/vorticity form of the above shallow-water set, as discussed in the appendix. The inclusion of hyperdiffusion terms to prevent spectral blocking is also discussed in the appendix. In the spectral method the horizontal structure of the dependent variables is represented by series expansions in terms of spherical harmonics $P_n^m(\sin\phi)e^{im\lambda}$, where P_n^m is the associated Legendre function, m the zonal wavenumber, and n the total wavenumber, with $0 \leq |m| \leq n$. The model uses triangular truncation $0 \leq n \leq N$, with $N = 213$.

The principle of conservation of potential vorticity is derived by combining (1)–(3) to obtain

$$\frac{DP}{Dt} = -\frac{PQ}{h}, \quad (5)$$

where the potential vorticity is given by

$$P = \left(\frac{\bar{h}}{h}\right)\zeta \quad (6)$$

and the material derivative by

$$\frac{D}{Dt} = \frac{\partial}{\partial t} + u\frac{\partial}{a\cos\phi\,\partial\lambda} + v\frac{\partial}{a\partial\phi}. \quad (7)$$

In (6), $\bar{h}$ is a constant mean initial depth, introduced so that the potential vorticity P has the same units as the absolute vorticity ζ. Equation (5) implies material conservation of potential vorticity in the absence of any mass sinks or sources.

The shallow-water model is a very useful simple tool to study tropical atmospheric phenomena that are dominated by horizontal advection of potential vorticity. In a linear, compressible atmosphere, it is possible to sep-

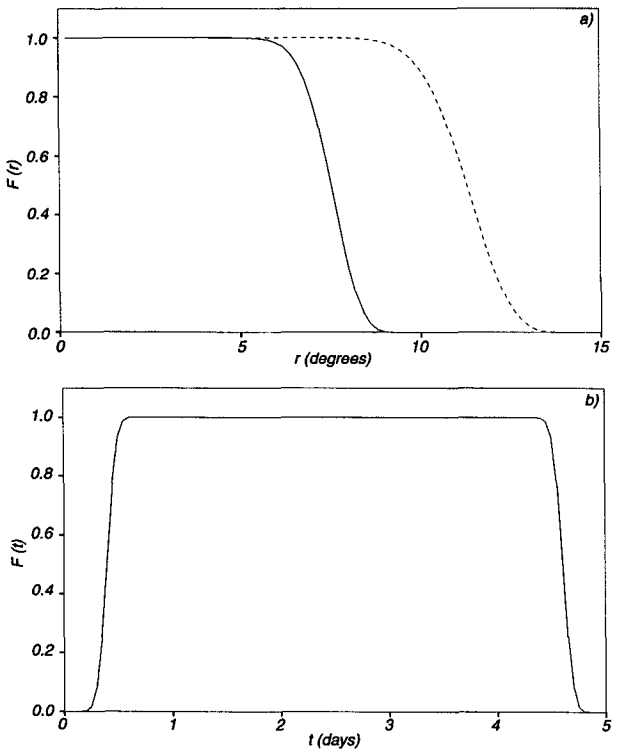

FIG. 3. Nondimensional radial, $\mathcal{F}[r(\lambda, 0), 30]$, and temporal, $\mathcal{F}[\tau(t), 320]$, structures of the mass sink as given by (12): (a) $\mathcal{F}[r(\lambda, 0), 30]$ corresponds to 10° zonal half-width (solid line), and $\mathcal{F}[r(0, \phi), 30]$ corresponds to 15° meridional half-width (dashed line); (b) $\mathcal{F}[\tau(t), 320]$ for $t_0 = 5$ days.

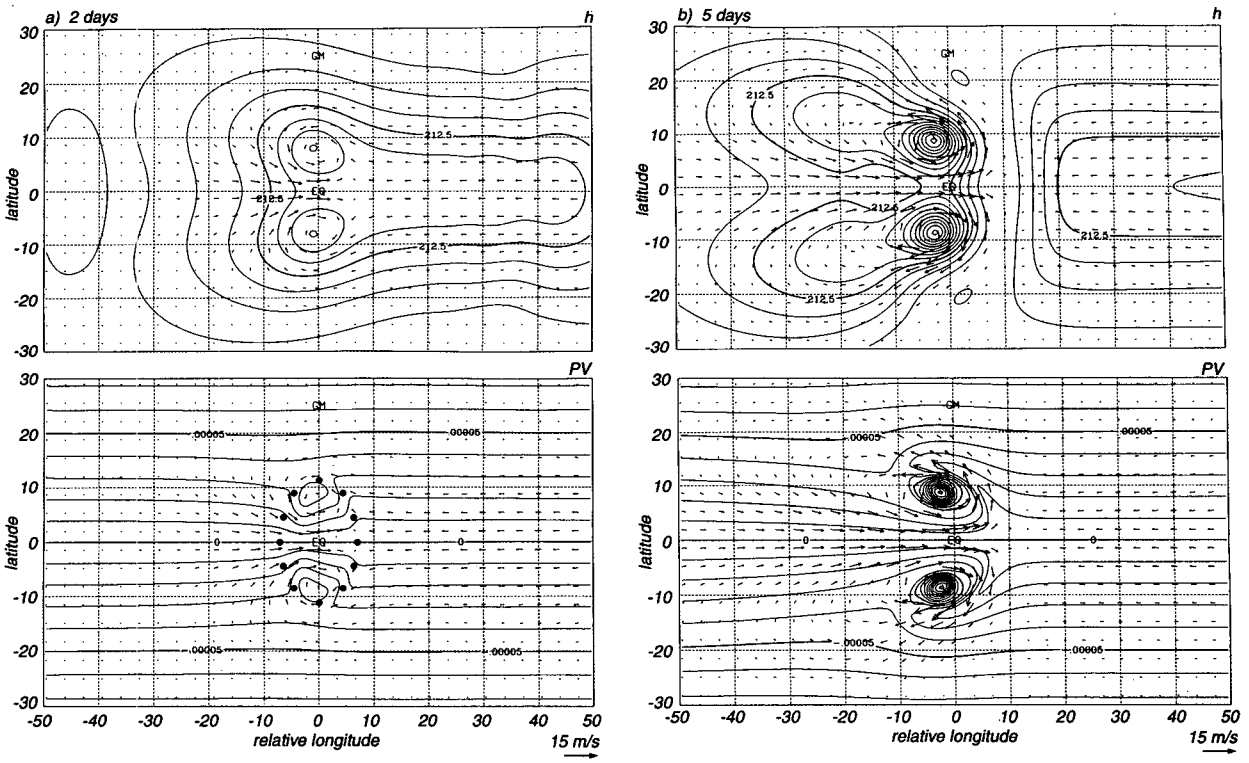

FIG. 4. Evolution of the flow field in response to a meridionally elongated mass sink centered at the equator. The mass sink has a duration of 5 days, and its shape and position are indicated by the dots in Fig. 4a. The displayed fields are the winds (m s^{-1}), fluid depth (m), and PV (s^{-1}) at (a) 2, (b) 5, and (c) 10 days.

arate the horizontal structure of motion from its vertical structure (Fulton and Schubert 1985). Such an atmosphere may then be seen as a linear combination of numerous sets of shallow-water equations with different equivalent depths ($\bar{h}$) and corresponding vertical structures. Several studies (e.g., Fulton and Schubert 1985) have shown that the tropical tropospheric response to organized convection is dominated by baroclinic modes whose equivalent depth ranges between 100 and 500 m. This allows the use of shallow-water models in the study of convectively forced tropical circulations (e.g., Gill 1980).

4. Twin cyclone formation with stationary mass sinks

In this section, the role of super cloud cluster convection in the formation of twin tropical disturbances is studied using the global nonlinear shallow-water model. In the model, super cloud cluster convection is simulated by a mass sink. According to (5), an imposed mass sink produces a positive potential vorticity (PV) anomaly in the Northern Hemisphere in a way that is analogous to the effect of convection upon the lower troposphere (e.g., Schubert et al. 1991). The mass sinks used in this study are highly idealized in the sense that they do not account for the existence of a hierarchy of convective scales in the MJO. A more realistic mass sink would produce finer-scale features in the PV field. However, the smoothing property of the elliptic operator in (A9) renders the flow field nearly insensitive to the details of the PV field.

The spatial and temporal variation of the mass sink are given by

$$Q(\lambda, \phi, t) = Q_0 \mathcal{F}[r(\lambda, \phi), 30] \mathcal{F}[\tau(t), 320], \quad (8)$$

where

$$\mathcal{F}(x, \gamma) = \begin{cases} 1, & \text{for } x = 0 \\ 1 - \exp\left[-\dfrac{\gamma}{x} \exp\left(\dfrac{1}{x-1}\right)\right] & \\ & \text{for } 0 < x < 1 \\ 0, & \text{otherwise}, \end{cases} \quad (9)$$

is a smooth unit step function, with $r(\lambda, \phi) = [(\lambda \cos\phi)^2/b^2 + (\phi - \phi_0)^2/c^2]^{1/2}$ and $\tau(t) = |2t/t_0 - 1|$. The constants ϕ_0, b, c, t_0, and Q_0, respectively determine the central latitude, zonal and meridional extents, duration, and magnitude of the forcing. The integrations shown in this section and section 5 are initialized with a state of rest and a constant fluid depth of 222 m (Fulton and Schubert 1985), which gives a

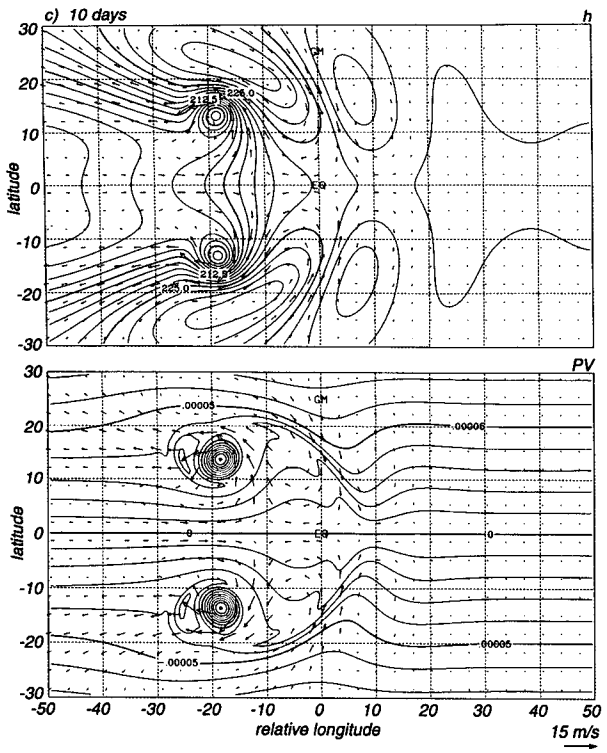

FIG. 4. (*Continued*)

gravity wave phase speed of 46.6 m s^{-1} and an equatorial Rossby length $[a(g\bar{h})^{1/2}/(2\Omega)]^{1/2}$ of 1427 km. The values of the specified constants are $b = \pi/18$ (10° zonal half-width), $c = \pi/12$ (15° meridional half-width), and $Q_0 = -82.8$ m day^{-1}. Two values of ϕ_0 will be used: $\phi_0 = 0$ (forcing centered at the equator) and $\phi_0 = \pi/72$ (forcing centered at 2.5°N). The steepness parameters determine the spatial ($\gamma = 30$) and temporal ($\gamma = 320$) scales over which the unit step is smoothed. Figure 3 summarizes the spatial and temporal structures of the mass sink. In order to obtain a reasonable timescale for the flow evolution, the value of Q_0 given above has been chosen to be consistent with Fulton and Schubert's (1985, Table 5) vertical normal-mode projections of ITCZ apparent heat source profiles. Over the entire simulation, this mass sink results in a 1% decrease in the initial globally integrated mass.

Figure 4 shows the temporal evolution of h, PV, and winds produced by the mass sink described above, when $\phi_0 = 0$ and $t_0 = 5$ days. After 2 days of simulation (Fig. 4a), a Kelvin wave signature dominates the flow to the east of the mass sink. In the region of the mass sink, two cyclonic PV anomalies on opposite sides of the equator are being produced through the $-PQ/h$ term in (5). Since this term vanishes at the equator, there is no PV anomaly produced there. Equatorial westerly winds occur in the region of the mass sink and to its west. The geopotential and wind fields at this time are very similar to the steady-state results obtained by Gill (1980). The two cyclones and the equatorial westerly winds will continue to intensify until the mass sink is turned off on day 5 of the simulation. Also note that a progressive tightening of equatorial PV isolines occurs for as long as the forcing is active.[3] When the mass sink is turned off at day 5 (Fig. 4b), the two cyclones straddling the equator and their associated equatorial westerlies attain their absolute intensity maxima of 1.3 $\times 10^{-4}$ s^{-1} and ~12 m s^{-1}, respectively. Once the mass sink is turned off, the two cyclones initiate their poleward and westward movement, and the Kelvin wave packet freely propagates eastward (see height field in Fig. 4b). In a sense, the twin cyclones emerge from the northwest and southwest edges of the idealized convective region. The poleward and westward movement of the twin cyclones is called β drift and is due to linear and nonlinear interactions between the cyclones and the meridionally varying planetary vorticity (e.g., Li and Wang 1994). As the twin cyclones move poleward, the strongest westerly winds become displaced away from the equator, and the equatorial tightening of the PV isolines is relaxed (Fig. 4c). Likewise, the leading edge of the equatorial westerlies follows the westerly movement of the twin cyclones. Dispersion of short Rossby wave energy produces the Rossby wave train seen to the east of the twin cyclones in the PV and height fields (Fig. 4c). Such dispersive effects of short Rossby waves are not reproduced in models that use the long-wave approximation (e.g., Gill 1980; Gill and Philips 1986). These effects are also distorted in models that use the β-plane approximation (Hoskins et al. 1977). During the simulation, the zero-PV line remains undisturbed, indicating that there is no interchange of mass between the two hemispheres. The evolution of the equatorial westerly winds is similar to the evolution of the westerly wind bursts associated with Supertyphoon Lola and Tropical Cyclone Namu and with the five-case composite of Chen (1993).

If the mass sink is rotated 90° around its axis so that it is elongated along the equator, the flow fields it produces (not shown) are weaker than those of the previous experiment. This is a consequence of applying a larger fraction of the mass sink at lower latitudes where the term $-PQ/h$ in (5) is least efficient.

A similar evolution is obtained when the center of the same mass sink is moved to 2.5°S (not shown). As expected, the results are no longer perfectly symmetric about the equator. The Southern Hemisphere cyclone is stronger than its Northern Hemisphere counterpart because a mass sink applied at larger $|f|$ is more efficient at producing a cyclonic circulation through the

[3] In the upper levels the opposite, that is, a gradual spreading of the PV isolines, would be expected. Interestingly, an equatorial spreading of the upper-tropospheric PV isolines is present in the ECMWF analyses during the boreal summer months in the west Pacific and Indian Oceans (Hoskins 1991).

$-PQ/h$ term in (5). The maximum intensity of the equatorial westerly winds is the same, but its center is shifted southward. As in the previous simulation, after the mass sink is turned off, the two cyclones begin to propagate westward and poleward, causing the equatorial westerlies to weaken and move westward. In this case, exchange of mass between the two hemispheres occurred with intrusion of negative PV air from the Southern into the Northern Hemisphere, and vice versa, producing regions in which the necessary condition for occurrence of inertial instability (namely that $fP < 0$) is met. However, inertially unstable modes have very slow growth rates for flows with a large $\bar{h}$ (Stevens 1983) and therefore are not apparent in any of the simulations shown here.

The foregoing experiments offer at least a qualitative picture of how twin tropical disturbances and WWBs may form in association with a stationary super cloud cluster that is independent of any MJO episodes [for instance, Tropical Cyclones Roger and Irma in March 1993, as described by Flatau et al. (1995)].

5. Twin cyclone formation with moving mass sinks

In this section, the shallow-water model is used to study the effects of super cloud cluster motion and intensity variations on the formation of the cyclonic circulations associated with twin tropical disturbances.

When the mass sink used in the previous section moves eastward at a constant speed, interesting results are obtained. The mass sink is initially centered at 0° latitude and 0° longitude and propagates eastward at a constant speed of 10 m s^{-1} until it is turned off at 5 days. Figure 5 shows the PV, height, and wind fields obtained at 5 days of simulation. Two zonally elongated PV extrema straddling the equator are produced in this case. The circulation patterns associated with each of these PV extrema resemble the monsoon trough circulation. When compared to the results obtained with the stationary mass sink (Fig. 4c), the circulations produced in this case (Fig. 5) are weaker (maximum equatorial westerlies of ~8 m s^{-1}) and extend ~40° farther east, covering a larger horizontal area. These results are expected since, when all other parameters are kept unchanged, an increase in the propagation speed of the mass sink results in an increase in the horizontal areas they affect, consequently weakening the circulations produced. The eastward movement of the leading edge of the equatorial westerlies accompanying the mass sink is consistent with observations of westerly winds trailing MJO convection (Nakazawa 1988).

The flow produced by the moving mass sink satisfies the necessary, but not sufficient, condition for barotropic instability to occur. This condition, strictly valid only for zonally symmetric unforced flow, is that $dP/d\phi < 0$ somewhere (Eliassen 1983; Ripa 1983), that is, that there exists the possibility of counterpropagating Rossby waves. Since the flows in this study are

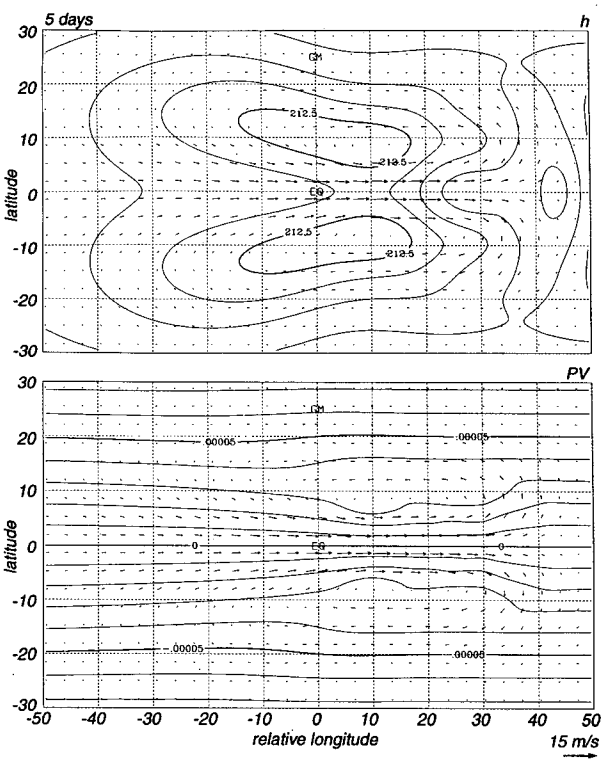

FIG. 5. Wind (m s^{-1}), PV (s^{-1}), and fluid depth (m) fields for a simulation in which a meridionally elongated mass sink centered at the equator is moving due east at 10 m s^{-1}. Results are for day 5 of the simulation.

forced and not zonally symmetric, the barotropic instability criterion should be taken only as a rough guide. The importance of forcing effects in barotropic instability conditions has been emphasized by Andrews (1984). In any event, even though $dP/d\phi < 0$ in certain regions, the rather weak shear regions in this experiment do not lead to any rapid or significant transformations in the flow regime (Kuo 1973).

A more realistic scenario for the effects of MJO convection upon the lower-tropospheric tropical circulation is obtained when the mass sink intensity and eastward speed vary in time according to the functions shown in Fig. 6. In that figure, mass sink intensity and eastward speed are normalized with respect to Q_0 and 10 m s^{-1}, respectively. Initially, the mass sink gradually intensifies while stationary at 0° relative longitude. Between days 3 and 13 the mass sink moves eastward, and its intensity reaches a minimum around day 8. After day 13 the mass sink is kept active for 2 more days while stationary near 72° relative longitude. These mass sink intensity and speed variations were chosen in order to simulate observations (Rui and Wang 1990; Wang and Rui 1990; Weickman and Khalsa 1990) that the MJO convection intensifies while almost stationary in the eastern equatorial Indian Ocean, weakens while moving eastward over the Maritime Continent, again

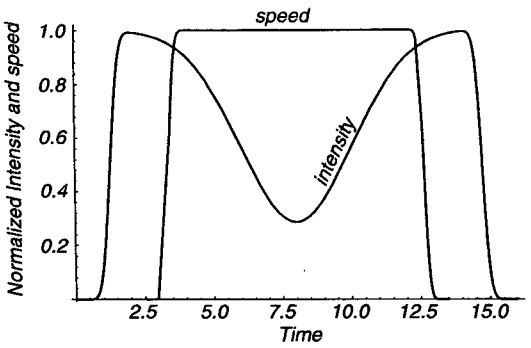

FIG. 6. Time variations of the mass sink intensity $\mathcal{F}[\tau(t), 320]$ and eastward speed (normalized with respect to 10 m s^{-1}).

intensifies once it reaches the west Pacific Ocean, and finally becomes stationary and dies off near the date line.

Figure 7 shows the evolution of the PV, wind, and height fields in response to the eastward moving mass sink of varying intensity described above. By day 4 (Fig. 7a), the mass sink has just started to slowly propagate eastward and is located near 5° relative longitude. The circulation pattern again consists of twin cyclones straddling the equator to the west of the mass sink and a Kelvin wave structure to the east. The maximum PV in the twin cyclones near 0° relative longitude has an absolute value of 6.0×10^{-5} s^{-1}. As the mass sink moves eastward, the twin cyclones remain near 0° relative longitude and two weaker zonally elongated PV extrema straddling the equator and associated equatorial westerlies are progressively produced. On day 8 of the simulation (Fig. 7b), the mass sink is located at 36° relative longitude, and its intensity is a minimum (Fig. 6). At this time, the equatorial westerlies and corresponding PV gradient tightening extend to near 34° relative longitude. The twin cyclones near 0° relative longitude begin to propagate poleward and westward after the mass sink intensity has dropped to a minimum at 8 days. Between days 13 and 15.5 the mass sink produces a second pair of PV extrema straddling the equator while stationary near 72° relative longitude (Fig. 6). Note that the equatorial westerly winds are stronger where the mass sink was nearly stationary than where the mass sink was moving due east. A similar trend exists in the winds that accompanied the MJO episode shown in Fig. 1. Although the time-integrated forcing was the same while the mass sink was stationary near 0° and 70° relative longitude, the easternmost cyclonic pair is somewhat weaker than the westernmost one (Fig. 7c). This occurs because near 0° relative longitude the mass sink is strongest after having produced two incipient cyclones, while near 70° relative longitude the mass sink is stronger when no cyclonic circulation is present. Since the efficiency of the mass sink in producing a cyclonic circulation is directly proportional to the strength of the cyclone (Schubert et al. 1980), the mass sink efficiency is greater near 0° than near 70° relative longitude. Between 0° and 65° relative longitude two zonally elongated cyclonic PV anomalies straddle the equator. The necessary condition for barotropic instability to occur is satisfied on the poleward side of these elongated PV anomalies, but instability, once again, fails to occur. After the mass sink is turned off, the second pair of cyclones also begins to propagate poleward and westward (see Fig. 7d at 20 days). Meanwhile, the tightening of the PV isolines near the equator is progressively relaxed, and the equatorial westerlies retreat to the west. In summary, this mass sink produced two pairs of cyclonic circulations straddling the equator in the two regions where it was stationary, namely near 0° and 70° relative longitude.

The MJO convection is observed to migrate across the equator twice a year, in the equinoxes. This motivates one last forced experiment in which the same eastward moving mass sink of variable intensity was centered at 2.5°S. The PV, wind, and mass fields obtained in this simulation (Fig. 8) evolve similarly to those in the previous experiment except for the effects of the asymmetries introduced by centering the mass sink away from the equator. At 4 days (Fig. 8a), a pair of cyclones straddles the equator near 0° relative longitude. The SH cyclone is centered at 9°S, and its extremum PV has an absolute value of 8.0×10^{-5} s^{-1}. The NH storm is centered closer to the equator, at 5°N, and its maximum PV absolute value, 5.0×10^{-5} s^{-1}, is weaker than that of the SH cyclone. The strongest equatorial westerlies (12 m s^{-1}) occur to the south of the equator in association with the strongest cyclone. Also, there is a net northerly flow across the equator between the two storms causing the zero-PV line in that region to be displaced into the SH. At 15 days (Fig. 8b), a second pair of cyclones has been produced by the mass sink while stationary near 70° relative longitude. This pair of cyclones is again weaker than the first pair initially was. The first pair of cyclones is now located westward and poleward of their initial positions near 0° relative longitude. In the region between −10° and 65° relative longitude, two elongated cyclonic PV anomalies straddle the equator. The elongated NH PV anomaly is centered near 7°N, and the SH elongated PV anomaly is stronger and centered near 11°S. Note that since the meridional gradient of PV is reversed on the poleward side of these elongated cyclonic PV anomalies (Fig. 8b), the necessary condition for barotropic instability is satisfied. In this case, small perturbations from zonal symmetry introduced by variations in the mass sink intensity cause undulation and breakdown of the elongated PV anomalies (Guinn and Schubert 1993), producing cyclones near 8°S, at 5° and 25° relative longitude, and near 4°N, at 12° and 45° relative longitude. During the Tropical Oceans and Global Atmosphere Coupled Ocean–Atmosphere Response Experiment, for instance, tropical disturbances occurred trailing the MJO convection as it crossed the Maritime Continent (see Fig. 8 of Chen et al. 1996). This sim-

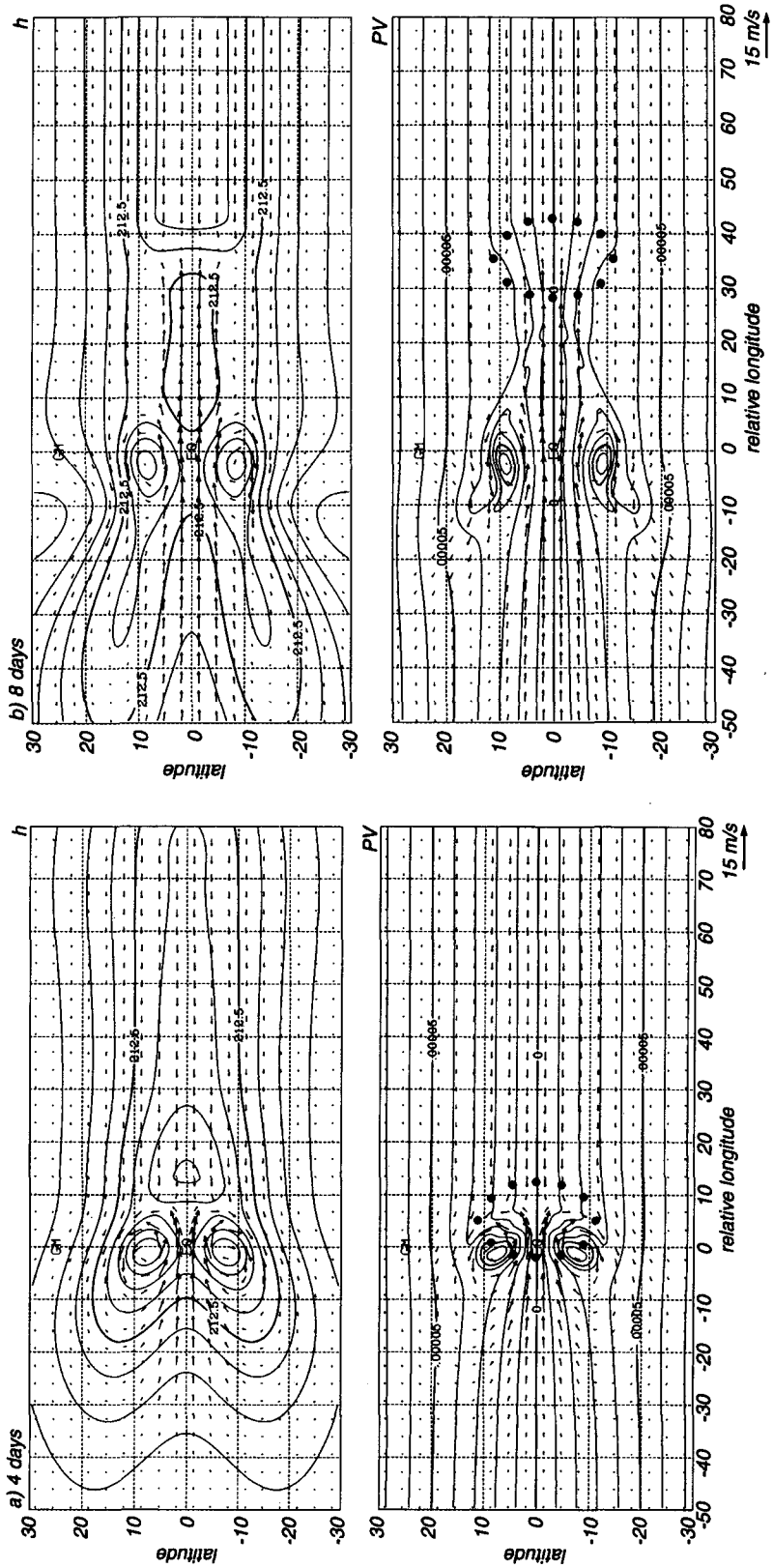

FIG. 7. Evolution of the PV (s^{-1}), fluid depth (m), and wind ($m\ s^{-1}$) fields in response to an equatorially centered, meridionally elongated mass sink whose intensity and eastward speed vary according to Fig. 5. The position and shape of the mass sink are indicated by the dots. Results are shown at (a) 4, (b) 10, (c) 15, and (d) 20 days.

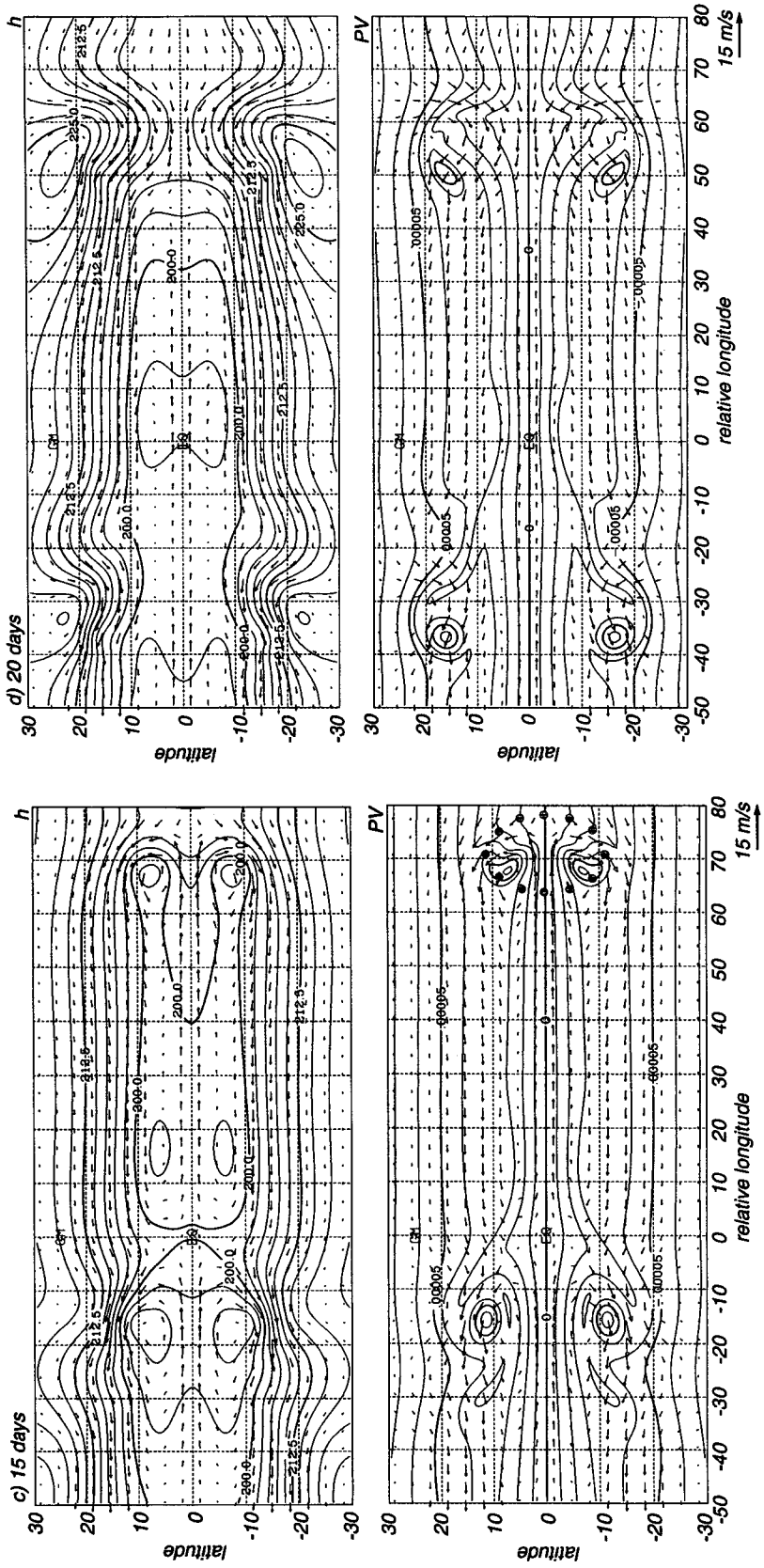

FIG. 7. (*Continued*)

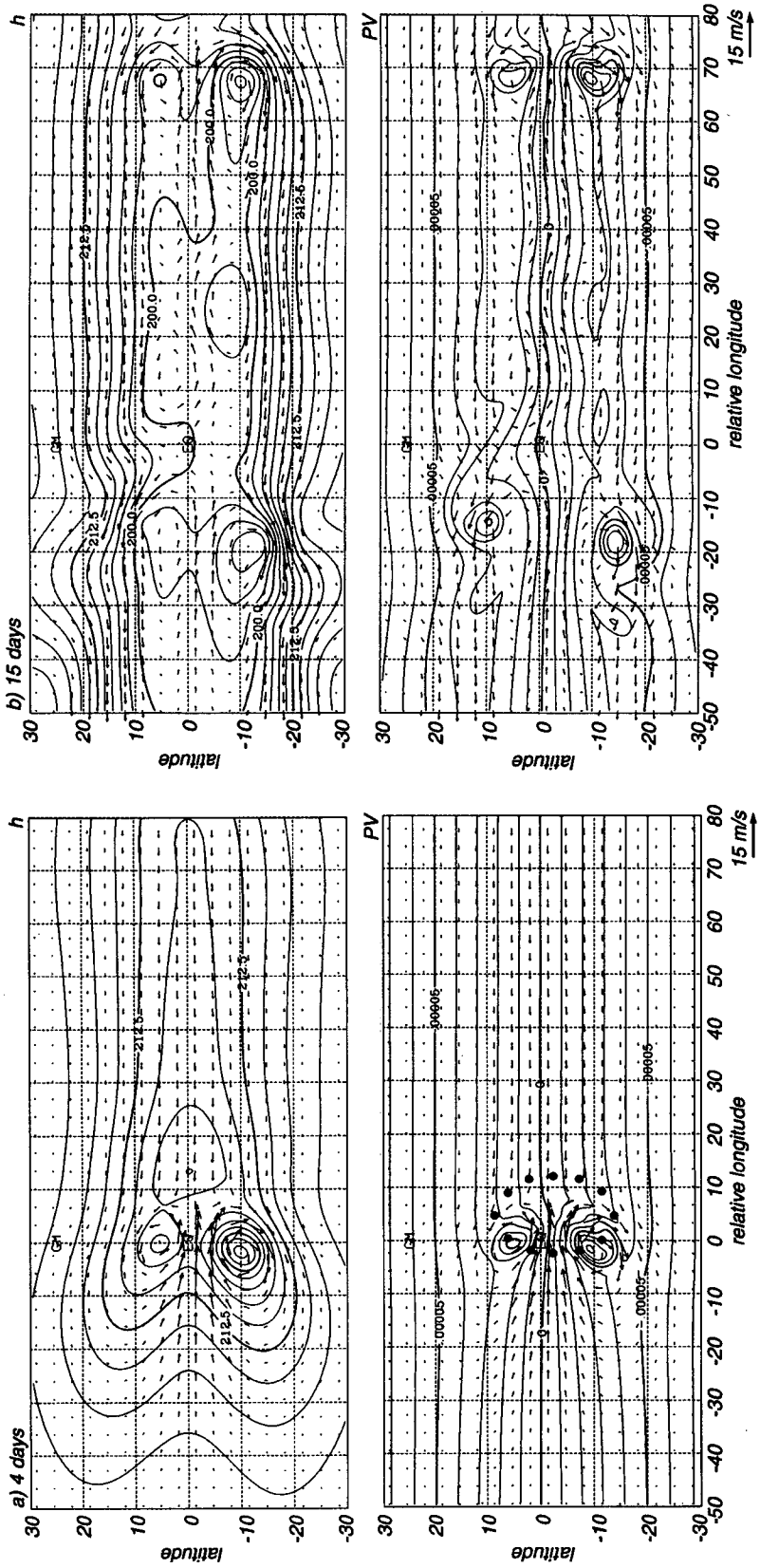

FIG. 8. Evolution of the PV (s^{-1}), fluid depth (m), and wind ($m\ s^{-1}$) fields in response to a mass sink centered at 2.5°S whose intensity and eastward speed vary according to Fig. 5. Results are shown at (a) 4 and (b) 15 days.

ulation points to the possibility that barotropic instability plays a role in the formation of these disturbances.

Despite the simplicity of these shallow-water simulations, the circulations they produce resemble those associated with the observed MJO. In particular, the production of equatorial westerly winds and cyclones by the mass sink in the model are similar to the formation and evolution of tropical disturbances and WWBs in association with the MJO (e.g., Nakazawa 1988).

6. Twin cyclone movement

One way to idealize the flow associated with twin tropical cyclones is as a pair of point vortices (of equal strength and opposite sign) described by nondivergent barotropic dynamics on a plane. Such an idealized flow (Batchelor 1967, section 7.3) is steady relative to axes that move at a constant speed in a direction normal to the line connecting the two vortices; in the relevant atmospheric case, the direction of movement is eastward. The speed of movement is directly proportional to the strength of the point vortices and inversely proportional to the distance between them. More general, steadily translating solutions also exist for smoothly distributed vorticity fields on the plane (Batchelor 1967, section 7.3). For nondivergent barotropic dynamics on the sphere, the mathematics is more complicated, but such solutions have been worked out in connection with modon theory (e.g., Tribbia 1984; Verkley 1987). In any event, these theoretical solutions prompt us to ask the following question. Can twin tropical cyclones ever become so strongly coupled that they simply propagate eastward as a vortex pair?

To help answer this question, we shall now perform several initial-value experiments to study the movement of twin cyclones in an otherwise resting atmosphere. In order to allow the initial mass and wind fields to be balanced, the mean fluid depth was changed to 4500 m. Nonlinear balance (Charney 1960) was initially assumed.

In a shallow-water flow on the sphere, the movement of a cyclone is dictated by β drift, advection by environmental steering flows, and the meridional relative vorticity gradient. The poleward and westward movement of cyclones is called β drift and is caused by linear and nonlinear interactions between the cyclone circulation and the meridionally varying planetary vorticity (e.g., Li and Wang 1994). The meridional gradient of relative vorticity acts to oppose β drift when its sign is opposite to the planetary vorticity gradient and to enhance it when they are of the same sign (Evans et al. 1991). Nonlinear effects are fundamental for cyclone movement in association with environmental and planetary vorticity gradient effects. In fact, in linear simulations cyclones tend to become zonally elongated due to Rossby wave energy dispersion, while their centers remain nearly stationary (Chan and Williams 1987).

Results obtained in four initial-value experiments will now be discussed. In the first experiment (SYM1), two cyclones of the same intensity (relative vorticity has an absolute value of $2 \times 10^{-4}\ s^{-1}$) and radius (2° latitude) are initially placed at 5°S and 5°N. Figure 9 shows a radial cross section of the tangential wind and vorticity in these cyclones. In the second experiment (SYM2), the same two cyclones are initially placed at 2.5°S and 2.5°N. In the third experiment (ASYM), the two cyclones are again placed at 5°S and 5°N, but the intensity of the southern one is halved. In the last experiment (VOR) the motion of a single cyclone in a quiescent environment centered at 5°N with a relative vorticity of $2 \times 10^{-4}\ s^{-1}$ and a radius of 2° latitude was calculated. This simulation is a reference to illustrate the effects of introducing a second cyclone in the SH.

Figure 10 shows the trajectories followed by the cyclones in the aforementioned experiments. The trajectory followed by the single cyclone in a resting environment (VOR) is north-northwestward, as dictated by β drift. The introduction of an identical cyclone to the south of the equator (SYM1) causes both cyclones to initially have an eastward movement component due to mutual advection by their associated equatorial westerlies. After 2 days, both cyclones move westward and poleward. Note, however, that their trajectories are longer and more zonal than that of the single cyclone (VOR). When the southern cyclone is only half as strong as the northern one (ASYM), their trajectories will also be longer and more zonal than that of the single cyclone (VOR), but they will no longer be symmetric about the equator. The SH cyclone initially moves to the east under the influence of the steering flow of the NH cyclone and after 3 days starts moving west-southwest. In this simulation the trajectory of the NH cyclone deviates less from VOR than the trajectory in SYM1 because the effect of the SH cyclone is weaker.

Experiments with increasingly larger distances between the two cyclones show that their mutual trajectory influence decreases with distance until they move independently, as dictated by pure β drift. On the other hand, if the two cyclones are initially placed at 2.5°S and 2.5°N (SYM2), their mutual steering flow makes them move due east. However, this behavior may never occur in nature because convection processes do not tend to produce cyclone pairs so close to the equator.

7. Concluding remarks

In this study a nonlinear shallow-water model on the sphere was used to investigate barotropic aspects of the formation of the horizontal circulations of tropical disturbances that trail MJO convection. The model was also used to study the movement of twin tropical cyclones.

In the model, an eastward moving, meridionally elongated mass sink was used to simulate the effects of

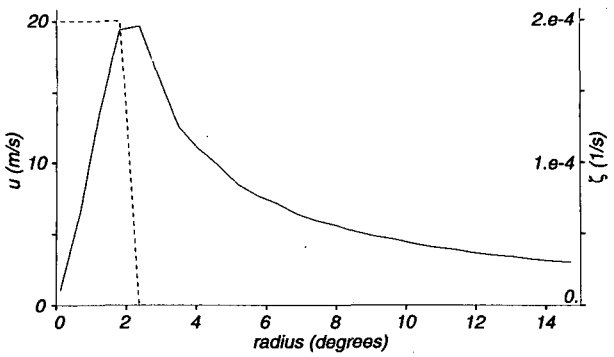

FIG. 9. Radial distributions of relative vorticity (s^{-1}) and tangential wind ($m\ s^{-1}$) for the cyclones used in the trajectory experiments shown in Fig. 10.

MJO convection in the lower troposphere. The mass sink intensity and speed variations were chosen to simulate observations that MJO convection intensifies while almost stationary in the eastern equatorial Indian Ocean, weakens while moving eastward over the Maritime Continent, again intensifies once it reaches the west Pacific Ocean, and finally becomes stationary and dies off near the date line. When centered at the equator, this mass sink produced twin cyclones in the two regions where it was stationary, namely, where it was initially turned on (near 0° relative longitude) and where it was turned off (near 70° relative longitude). A broad region of equatorial westerly winds was produced trailing the mass sink with the strongest winds in the two regions where twin cyclones were produced. In addition, the mass sink produced two weaker zonally elongated cyclonic PV anomalies straddling the equator in the region where it propagated eastward, namely, between 0° and 65° relative longitude. Although the flow associated with these elongated PV anomalies satisfies the necessary condition for barotropic instability to occur, it does not become unstable, possibly because the growth rates of unstable modes for such weak shear regions are very small.

Given that the MJO convection is not always centered at the equator, another simulation was run with the mass sink displaced to 2.5°S. Once again, twin cyclones were produced near 0° and 70° relative longitude where the mass sink was stationary, and zonally elongated cyclonic PV anomalies were produced in the region where the mass sink propagated eastward. This mass sink produced the strongest cyclones and PV anomalies in the SH. Consequently, the maximum equatorial westerly winds occurred in the SH. In this simulation, the elongated cyclonic PV anomalies straddling the equator undulated and broke down due to barotropic instability, producing four weak cyclones.

The evolution of the circulations produced in these simulations resemble the evolution of the low-level circulations associated with the MJO (Fig. 1). In particular, the development of cyclones and equatorial westerly winds in the model are reminiscent of the formation and evolution of tropical disturbances and WWBs in association with MJO convection. Note, however, that the observed intensification of the equatorial westerlies as twin tropical cyclones develop has no counterpart in this simple model. The cyclones formed in the simulations shown here are far from the intensity of tropical cyclones and would require a substantial diabatic boost in their PV to reach such intensity.

It is proposed that MJO convection may produce twin tropical disturbances in the two regions where it is stationary, namely its region of formation in the eastern Indian Ocean and its region of decay near the date line. In the west Pacific Ocean in particular, observations indicate that twin tropical cyclones preferentially occur near the date line (Ogura and Chen 1987). The model results indicate that the intensity of the tropical disturbances and other circulations produced depends on the intensity and central latitude of MJO convection. The model results also suggest that the observed formation of tropical disturbances as MJO convection crosses the Maritime Continent may be due to instability of the elongated cyclonic PV anomalies that trail the convection. A comprehensive climatology of tropical cyclone formation in association with the MJO is needed to verify this hypothesis.

Finally, the movement of twin tropical cyclones was studied in a series of initial value experiments in which two cyclones were placed on opposite sides of the equator. Each cyclone influences the trajectory of the other through changes in the steering flow and meridional PV gradient. The relative importance of these effects remains to be studied. Nonlinear effects are very important in the study of twin cyclone motion since the steer-

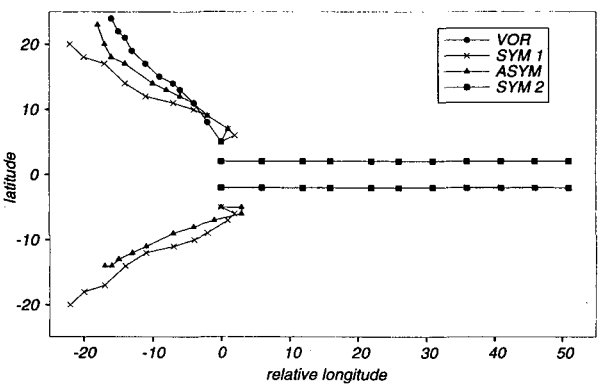

FIG. 10. Trajectories followed by twin cyclones in initial value experiments with the shallow-water model. Two 2° radius cyclones whose $\zeta = 2 \times 10^{-4}\ s^{-1}$ initially centered at 5°S and 5°N followed the trajectory labeled as SYM1. In SYM2 the same two cyclones were centered at 2°S and 2°N. In the asymmetric case (ASYM) the northern cyclone has the same characteristics as the ones in SYM1 and is twice as intense as the southern cyclone. The trajectory followed by a single cyclone (VOR) whose initial characteristics are the same as the vortices in SYM1 is also shown (VOR) for comparison. Marks along each 10-day trajectory are 1 day apart.

ing flows and environmental PV continue to change as the cyclones move. The mutual interaction between the two cyclones causes their trajectories to be longer and more zonal than that dictated by β drift. When the two cyclones are placed 2.5° away from the equator, they are advected due east by the equatorial westerlies between them. This behavior, however, may never occur in nature, because convection processes do not tend to produce cyclone pairs so close to the equator.

Acknowledgments. We have benefited greatly from the comments of Paul Ciesielski, William Gray, Richard Johnson, Michael Montgomery, David Randall, Thomas Rickenbach, Richard Taft, Gerald Taylor, Raymond Zehr, and three anonymous reviewers. The present research was supported by CNPq, the Brazilian Council for the Development of Science and Technology, and by NOAA through TOGA COARE Grant NA37RJ0202.

APPENDIX

Divergence/Vorticity Form and Initialization of the Shallow-Water Model

Equations (1)–(3) form a closed system in u, v, and h. An equivalent closed system in δ, ζ, and h is obtained by replacing the momentum equations with the divergence and vorticity equations. This divergence/vorticity form of the equations of motion is the form integrated in the model. The divergence, vorticity, and continuity equations with the diffusion terms included are

$$\frac{\partial \delta}{\partial t} - \frac{\partial(\zeta V)}{a(1-\mu^2)\partial\lambda} + \frac{\partial(\zeta U)}{a\partial\mu} + \nabla^2\left[gh + \frac{U^2+V^2}{2(1-\mu^2)}\right] = -K\left(\nabla^4\delta - \frac{4}{a^4}\delta\right), \quad \text{(A1)}$$

$$\frac{\partial \zeta}{\partial t} + \frac{\partial(\zeta U)}{a(1-\mu^2)\partial\lambda} + \frac{\partial(\zeta V)}{a\partial\mu} = -K\left(\nabla^4\zeta - \frac{4}{a^4}\zeta\right), \quad \text{(A2)}$$

$$\frac{\partial h}{\partial t} + \frac{\partial(hU)}{a(1-\mu^2)\partial\lambda} + \frac{\partial(hV)}{a\partial\mu} = Q - K\nabla^4 h, \quad \text{(A3)}$$

where K is a hyperdiffusion coefficient and

$$\delta = \frac{\partial U}{a(1-\mu^2)\partial\lambda} + \frac{\partial V}{a\partial\mu}, \quad \text{(A4)}$$

$$\zeta = 2\Omega\mu + \frac{\partial V}{a(1-\mu^2)\partial\lambda} - \frac{\partial U}{a\partial\mu}, \quad \text{(A5)}$$

with $U = u\cos\phi$, $V = v\cos\phi$, and $\mu = \sin\phi$. Hyperdiffusion is added to control spectral blocking (i.e., accumulations on the smallest resolved scales); the undifferentiated terms on the right-hand sides of (A1) and (A2) prevent damping of solid body rotation.

The horizontal velocity may be written as the sum of a rotational part plus a divergent part; that is,

$$U = \frac{\partial \chi}{a\partial\lambda} - (1-\mu^2)\frac{\partial \psi}{a\partial\mu}, \quad \text{(A6)}$$

$$V = \frac{\partial \psi}{a\partial\lambda} + (1-\mu^2)\frac{\partial \chi}{a\partial\mu}, \quad \text{(A7)}$$

where ψ and χ are a scalar streamfunction and velocity potential, respectively. The prognostic variables δ and ζ can be expressed as functions of ψ and χ by substituting (A6) and (A7) into (A4) and (A5) to obtain

$$\delta = \nabla^2\chi, \quad \text{(A8)}$$

$$\zeta = 2\Omega\mu + \nabla^2\psi. \quad \text{(A9)}$$

The use of (A8) and (A9) eases matters because the Laplacian operator has a simple form in the spectral space whose basis functions are spherical harmonics.

Substitution of (A6)–(A9) into (A1)–(A3) yields a nonlinear system of prognostic equations for ψ, χ, and h that will be solved using the spectral transform method in space and semi-implicit time differencing. In order to start the integration in time, initial fields of either ζ, δ, and h or U, V, and h on the transform grid are required. For each time step the model calculates all nonlinear terms and diabatic processes on the transform grid. It then transforms all variables into spectral space where the linear terms, derivatives, and time tendencies are evaluated. Finally, all variables are transformed back to physical space, and one cycle of the integration is completed. For more information on the numerical aspects of the model, see Hack and Jakob (1992).

Time integration of the shallow-water model requires knowledge of the initial mass and momentum fields. Initialization of the model is straightforward in cases where the initial wind fields are at rest and the fluid depth is constant. If the initial state is not at rest, the model should be initialized with balanced mass and wind fields in order to keep transient gravity waves to a minimum. In the model simulations shown here, given the initial vorticity, the wind and geopotential fields are obtained therefrom as follows. First, the streamfunction ψ is obtained from the vorticity through (A9). The corresponding nondivergent wind field is then computed from

$$U = -(1-\mu^2)\frac{\partial \psi}{a\partial\mu} \quad \text{and} \quad V = \frac{\partial \psi}{a\partial\lambda}. \quad \text{(A10)}$$

At this point, it is assumed that the mass and wind fields obey a nonlinear balance relation that is obtained by neglecting the hyperdiffusion and the local time derivative of divergence in (A1), resulting in

$$g\nabla^2 h = \frac{\partial(V\zeta)}{a(1-\mu^2)\partial\lambda} - \frac{\partial(U\zeta)}{a\partial\mu} - \nabla^2\left[\frac{U^2+V^2}{2(1-\mu^2)}\right]. \quad \text{(A11)}$$

In summary, given an initial vorticity field, (A9) is used to compute the initial ψ, (A10) to compute the initial U and V, and (A11) to compute the initial h. The nonlinear terms in these equations are calculated in physical space, and the remaining terms are most easily computed in spectral space.

The value chosen for the hyperdiffusion coefficient is $K = 8.0 \times 10^{12}$ m^4 s^{-1}. This choice is sufficient to prevent spectral blocking and to give a reasonably straight tail to the kinetic energy spectra (Jakob-Chien et al. 1995). It results in a damping time of 27.5 h for the $n = 213$ spherical harmonic coefficients and a damping time of 444 h for the $n = 106$ coefficients. These damping rates are small enough that it is probably useful to view the flow simulations as essentially conservative except for the mass source/sink term Q.

REFERENCES

Andrews, D. G., 1984: On the stability of forced non-zonal flows. *Quart. J. Roy. Meteor. Soc.*, **110,** 657–662.

Batchelor, G. K., 1967: *An Introduction to Fluid Dynamics.* Cambridge University Press, 615 pp.

Bladé, I., and D. L. Hartmann, 1993: Tropical intraseasonal oscillations in a simple nonlinear model. *J. Atmos. Sci.*, **50,** 2922–2939.

Chan, J. C. L., and R. T. Williams, 1987: Analytical and numerical studies of the beta-effect in tropical cyclone motion. Part I: Zero mean flow. *J. Atmos. Sci.*, **44,** 1257–1265.

Charney, J. G., 1960: Integration of the primitive and balance equations. *Proc. Int. Symp. on Numerical Weather Prediction,* Tokyo, Japan, Meteor. Soc. Japan, 131–152.

Chen, S. S., 1993: Equatorial westerly wind bursts and double cyclones. Preprints, *20th Conf. on Hurricanes and Tropical Meteorology,* San Antonio, TX, Amer. Meteor. Soc., 615–617.

——, R. A. Houze, and B. E. Mapes, 1996: Multiscale variability of deep convection in relation to large-scale circulation in TOGA COARE. *J. Atmos. Sci.,* in press.

Eliassen, A., 1983: The Charney–Stern theorem on barotropic–baroclinic instability. *Pure Appl. Geophys.*, **121,** 563–572.

Evans, J. L., G. J. Holland, and R. L. Elsberry, 1991: Interactions between a barotropic vortex and an idealized subtropical ridge. Part I: Vortex motion. *J. Atmos. Sci.*, **48,** 301–314.

Flatau, M., P. Flatau, R. Nieto Ferreira, and P. A. Phoebus, 1995: The analysis of the development of a cyclone pair during CEPEX. Preprints, *21th Conf. on Hurricanes and Tropical Meteorology,* Miami, FL, Amer. Meteor. Soc., 413–415.

Fulton, S. R., and W. H. Schubert, 1985: Vertical normal mode transforms: Theory and application. *Mon. Wea. Rev.*, **113,** 647–658.

Giese, B. S., and D. E. Harrison, 1991: Eastern equatorial Pacific response to three composite westerly wind types. *J. Geophys. Res.*, **96,** 3239–3248.

Gill, A. E., 1980: Some simple solutions for heat-induced tropical circulation. *Quart. J. Roy. Meteor. Soc.*, **106,** 447–462.

——, and P. J. Philips, 1986: Nonlinear effects on heat-induced circulation of the tropical atmosphere. *Quart. J. Roy. Meteor. Soc.*, **112,** 69–91.

Gray, W. M., 1979: Hurricanes: Their formation, structure and likely role in the tropical circulation. *Supplement to Meteorology Over the Tropical Oceans,* D. B. Shaw, Ed., Royal Meteorological Society, 155–218.

Guinn, T. A., and W. H. Schubert, 1993: Hurricane spiral bands. *J. Atmos. Sci.*, **50,** 3380–3403.

Hack, J. J., and R. Jakob, 1992: Description of a global shallow water model based on the transform method. NCAR Tech. Note NCAR/TN-343+STR, 39 pp. [Available from Climate and Global Dynamics Division, NCAR, P.O. Box 3000, Boulder, CO 80307.]

Harrison, D. E., and B. S. Giese, 1991: Episodes of surface westerly winds as observed from islands in the western tropical Pacific. *J. Geophys. Res.*, **96,** 3221–3237.

Hartten, L. M., 1996: Synoptic settings of westerly wind bursts. *J. Geophys. Res.,* in press.

Hayashi, Y., and D. G. Golder, 1993: Tropical 40–50- and 25–30-day oscillations appearing in realistic and idealized GFDL climate models and the ECMWF dataset. *J. Atmos. Sci.*, **50,** 464–494.

Hoskins, B. J., 1991: Towards a PV–θ view of the general circulation. *Tellus,* **43AB,** 27–35.

——, A. J. Simmons, and D. G. Andrews, 1977: Energy dispersion in a barotropic atmosphere. *Quart. J. Roy. Meteor. Soc.*, **103,** 553–567.

Hsu, H.-H., B. J. Hoskins, and F.-F. Jin, 1990: The 1985/86 intraseasonal oscillation and the role of the extratropics. *J. Atmos. Sci.*, **47,** 823–839.

Hu, Q., and D. A. Randall, 1994: Low-frequency oscillations in radiative–convective systems. *J. Atmos. Sci.*, **51,** 1089–1099.

Jakob-Chien, R. J., J. J. Hack, and D. L. Williamson, 1995: Spectral transform solutions to the shallow water test set. *J. Comput. Phys.*, **119,** 164–187.

JTWC, 1986: Annual Tropical Cyclone Report Joint Typhoon Warning Center, U.S. Naval Oceanography Command Center, 238 pp. [Available from COMNAVMARIANAS Box 17, FPO, San Francisco, CA 96630.]

Keen, R. A., 1982: The role of cross-equatorial tropical cyclone pairs in the Southern Oscillation. *Mon. Wea. Rev.*, **110,** 1405–1416.

——, 1988: Equatorial westerlies and the Southern Oscillation. *Proc. U.S. TOGA Western Pacific Air–Sea Interaction Workshop,* Honolulu, HI, 121–140. [Available from UCAR Projects Office, P.O. Box 3000, Boulder, CO 80307.]

Kindle, J., and P. Phoebus, 1995: The ocean response to operational westerly wind bursts during the 1991–1992 El Niño. *J. Geophys. Res. Oceans,* **100,** 4893–4971.

Kingston, G., 1986: The Australian tropical cyclone season 1985–1986. *Aust. Meteor. Mag.*, **34,** 103–115.

Kuma, K., 1994: The Madden and Julian oscillation and tropical disturbances in an aqua-planet version of JMA global model with T63 and T159 resolution. *J. Meteor. Soc. Japan,* **72,** 147–172.

Kuo, H. L., 1973: Dynamics of quasi-geostrophic flows and instability theory. *Adv. Appl. Mech.*, **13,** 247–330.

Lander, M. A., 1990: Evolution of the cloud pattern during the formation of tropical cyclone twins symmetrical with respect to the equator. *Mon. Wea. Rev.*, **118,** 1194–1202.

Lau, K. M., L. Peng, C. H. Sui, and T. Nakazawa, 1989: Dynamics of super cloud clusters, westerly wind bursts, 30–60 day oscillations and ENSO: An unified view. *J. Meteor. Soc. Japan,* **67,** 205–219.

——, T. Nakazawa, and C. H. Sui, 1991: Observations of cloud cluster hierarchies over the tropical Western Pacific. *J. Geophys. Res.*, **96**(Suppl.), 3197–3208.

Li, X., and B. Wang, 1994: Barotropic dynamics of the beta gyres and beta drift. *J. Atmos. Sci.*, **51,** 746–756.

Liebmann, B., H. H. Hendon, and J. D. Glick, 1994: The relationship between tropical cyclones of the Western Pacific and Indian Oceans and the Madden–Julian oscillation. *J. Meteor. Soc. Japan,* **72,** 401–412.

Love, G., 1985: Cross-equatorial influence of winter hemisphere subtropical cold surges. *Mon. Wea. Rev.*, **113,** 1487–1498.

Luther, D. S., D. E. Harrison, and R. A. Knox, 1983: Zonal winds in the Central Equatorial Pacific and El Niño. *Science,* **222,** 327–330.

Madden, R. A., and P. R. Julian, 1971: Detection of a 40–50 day oscillation in the zonal wind in the tropical Pacific. *J. Atmos. Sci.*, **28,** 702–708.

——, and ——, 1994: Observations of the 40–50-day tropical oscillation—A review. *Mon. Wea. Rev.*, **122,** 814–837.

Mapes, B., and R. A. Houze, 1993: Cloud clusters and superclusters over the oceanic warm pool. *Mon. Wea. Rev.*, **121,** 1398–1415.

Miller, L., R. E. Cheney, and B. C. Douglas, 1988: GEOSAT altimeter observations of Kelvin waves and the 1986–1987 El Niño. *Science,* **239,** 52–54.

Nakazawa, T., 1988: Tropical super clusters within intraseasonal variations over the Western Pacific. *J. Meteor. Soc. Japan,* **66,** 823–839.

Nitta, T., 1989: Development of a twin cyclone and westerly bursts during the initial phase of the 1986–87 El Niño. *J. Meteor. Soc. Japan,* **67,** 677–681.

——, and T. Motoki, 1987: Abrupt enhancement of convective activity and low-level westerly burst during the onset phase of the 1986–87 El Niño. *J. Meteor. Soc. Japan,* **65,** 497–506.

Ogura, Y., and H.-N. Chin, 1987: A case study of cross-equatorial twin vortices over the Pacific in the northern winter using FGGE data. *J. Meteor. Soc. Japan,* **65,** 669–674.

Raymond, D. J., 1993: Westerly wind bursts in the Western Equatorial Pacific: An air–sea interaction instability? Preprints, *20th Conf. on Hurricanes and Tropical Meteorology,* San Antonio, TX, Amer. Meteor. Soc., 16–19.

Ripa, P., 1983: General stability conditions for zonal flows in a one-layer model on the β-plane or the sphere. *J. Fluid Mech.,* **126,** 463–489.

Rui, H., and B. Wang, 1990: Development characteristics and dynamic structure of tropical intraseasonal convection anomalies. *J. Atmos. Sci.,* **47,** 357–379.

Salby, M. L., and H. H. Hendon, 1994: Intraseasonal behavior of clouds, temperature, and motion in the Tropics. *J. Atmos. Sci.,* **51,** 2207–2224.

Schubert, W. H., J. J. Hack, P. L. Silva Dias, and S. R. Fulton, 1980: Geostrophic adjustment in an axisymmetric vortex. *J. Atmos. Sci.,* **37,** 1464–1484.

——, P. E. Ciesielski, D. E. Stevens, and H. Kuo, 1991: Potential vorticity modeling of the ITCZ and the Hadley circulation. *J. Atmos. Sci.,* **48,** 1493–1509.

Stevens, D. E., 1983: On symmetric stability and instability of zonal mean flows near the equator. *J. Atmos. Sci.,* **40,** 882–893.

Sui, C. H., and K. M. Lau, 1992: Multiscale phenomena in the tropical atmosphere over the western Pacific. *Mon. Wea. Rev.,* **120,** 407–430.

Tribbia, J. J., 1984: Modons in spherical geometry. *Geophys. Astrophys. Fluid Dyn.,* **30,** 131–168.

Verkley, W. T. M., 1987: Stationary barotropic modons in westerly background flows. *J. Atmos. Sci.,* **44,** 2383–2398.

Wang, B., and H. Rui, 1990: Synoptic climatology of transient tropical intraseasonal convective anomalies. *Meteor. Atmos. Phys.,* **44,** 43–61.

Weickmann, K. M., 1991: El Niño/Southern Oscillation and Madden–Julian (30–60 day) Oscillations during 1981–1982. *J. Geophys. Res.,* **96,** 3187–3195.

——, and S. J. S. Khalsa, 1990: The shift of convection from the Indian Ocean to the Western Pacific Ocean during a 30–60 day oscillation. *Mon. Wea. Rev.,* **118,** 964–978.

Yamagata, T., and Y. Hayashi, 1984: A simple diagnostic model for the 30–50 day oscillation in the tropics. *J. Meteor. Soc. Japan,* **62,** 709–717.

Yasunari, T., 1979: Cloudiness fluctuations associated with the Northern Hemisphere summer monsoon. *J. Meteor. Soc. Japan,* **57,** 227–242.

Zehr, R. M., 1993: Recognition of mesoscale vortex initiation as stage one of tropical cyclogenesis. Preprints, *20th Conf. on Hurricanes and Tropical Meteorology,* San Antonio, TX, Amer. Meteor. Soc., 405–408.